Complex Ordered Patterns in Mechanical Instability Induced Geometrically Frustrated Triangular Cellular Structures

Sung Hoon Kang,[1] Sicong Shan,[1] Andrej Košmrlj,[2] Wim L. Noorduin,[1] Samuel Shian,[1]
James C. Weaver,[3] David R. Clarke,[1] and Katia Bertoldi[1,4,*]

[1]*School of Engineering and Applied Sciences, Harvard University, Cambridge, Massachusetts 02138, USA*
[2]*Department of Physics, Harvard University, Cambridge, Massachusetts 02138, USA*
[3]*Wyss Institute for Biologically Inspired Engineering, Harvard University, Cambridge, Massachusetts 02138, USA*
[4]*Kavli Institute, Harvard University, Cambridge, Massachusetts 02138, USA*
(Received 5 December 2013; published 5 March 2014)

Geometrical frustration arises when a local order cannot propagate throughout the space because of geometrical constraints. This phenomenon plays a major role in many systems leading to disordered ground-state configurations. Here, we report a theoretical and experimental study on the behavior of buckling-induced geometrically frustrated triangular cellular structures. To our surprise, we find that buckling induces complex ordered patterns which can be tuned by controlling the porosity of the structures. Our analysis reveals that the connected geometry of the cellular structure plays a crucial role in the generation of ordered states in this frustrated system.

A geometrically frustrated system cannot simultaneously minimize all interactions because of geometric constraints [1,2]. The origin of this phenomenon can be easily illustrated by looking at the arrangement of spins with antiferromagnetic interactions on a triangle. In contrast to the case of a square, each spin on a triangle cannot be antialigned with all of its neighbors [see Fig. 1(a)]. Therefore, the system is frustrated and is characterized by degenerate ground states [3]. Given the difficulty of probing individual spin states in a system without disrupting their states [4], a number of artificial frustrated systems with individual discrete elements that can be directly monitored have been investigated to understand how spins accommodate the frustration of their interactions. These include artificial spin ice systems [4–11], colloid systems [2,12,13], and periodically arranged magnetic rotors [14]. Since geometrical frustration typically gives rise to disordered configurations, there has been growing interest in investigating mechanisms to generate order in frustrated systems. Interestingly, it has been reported that ordered configurations can be achieved either by introducing long-range interactions or lifting the geometrical constraints. In fact, the ordering of both pyrochlore magnets [15] such as $Ho_2Ti_2O_7$ and $Dy_2Ti_2O_7$ and artificial spin ice [11] is attributed to long-range dipolar interactions [3,16,17]. In addition, ordered configurations have been achieved by introducing dopants or defects [18,19] and distorting the lattice [2,20,21] to relax the geometrical constraints.

Here, we report a system consisting of elastic beams connected to form a two-dimensional triangular lattice in which a simple and ubiquitous phenomenon such as buckling [22] induces geometrical frustration. The essence

of this phenomenon can be easily captured by comparing a square and a triangular frame, as shown in Fig. 1(b). In the unfrustrated square frame each beam can buckle into the most energetically favored configuration—a half sinusoid—and simultaneously preserve the angles with all its neighbors at the joints to minimize the deformation energy. On a triangular frame, however, such configurations are impossible, so the system becomes frustrated. Then, what kind of patterns induced by buckling would appear in a triangular cellular structure? Interestingly, we show both numerically and experimentally that buckling in frustrated triangular cellular structures results in the formation of complex ordered patterns.

To understand patterns emerging as the result of buckling in a triangular cellular structure, we began by analytically
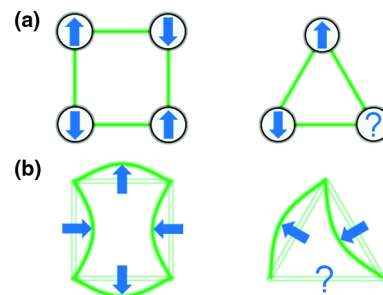

FIG. 1 (color online). Geometrical frustration. (a) In antiferromagnetic systems nearest neighbor spins want to align in opposite directions. This rule can be easily satisfied on a square. However, due to geometrical frustration it is not possible to satisfy it on a triangle. (b) Similarly, buckled beams on frames want to preserve angles at joints to minimize the deformation energy. Again this can be realized for square frames, but not for frustrated triangular frames.

investigating the stability of a single triangular frame consisting of three elastic beams of bending stiffness EI and length L, rigidly connected to each other, so that their relative orientation was fixed. Assuming that the beams were slender so that the contribution of the shear forces could be neglected, we used the stiffness matrix of a beam column [23] and imposed equilibrium conditions at each joint to determine the critical load and the corresponding modes (see Supplemental Material [24] for details). The analysis revealed that if all the three beams experienced the same compressive force P, the frame buckles as early as $P = 14.87(EI/L^2)$, leading to the formation of patterns for which

$$\theta_A + \theta_B + \theta_C = 0, \tag{1}$$

where θ_A, θ_B, and θ_C denote the rotation of the three junctions [see Fig. 2(a)]. Therefore, this simple analysis confirmed that buckling introduces degeneracy, since there are an infinite number of modes satisfying Eq. (1), ranging from a symmetric pattern with $\theta_B = 0$ and $\theta_A = -\theta_C$ to a chiral configuration with $\theta_A = -2\theta_C$ and $\theta_B = \theta_C$ [see Fig. 2(a) and Fig. S3].

We next performed finite element (FE) simulations to investigate the patterns induced by buckling in finite size periodic triangular cellular structure. We built two-dimensional models consisting of different numbers of unit cells [here we considered a unit cell composed of two adjacent triangles, see Fig. 2(c)] and investigated the stability of the system under equibiaxial compression using the commercial finite element package ABAQUS. We used a linear perturbation procedure to predict the critical strains (eigenvalues) associated with various buckled configurations (eigenmodes) and we expected the observed buckled configuration to be the one with the smallest critical strain. We find that the system—independent of its size and porosity—is characterized by two eigenmodes with very close critical strains [the critical strain difference is less than 0.1% for the 11×12 unit cells shown in Fig. 2(b). See also Tables S1—S3 in the Supplemental Material [24]]. Interestingly, if we focus on the center part of the models, which is only minimally influenced by edge effects, we see that both eigenmodes are characterized by ordered patterns with a periodic unit consisting of 3×3 unit cells, as shown in Fig. 2(b) for a structure with 11×12 unit cells.

Recognizing that the finite-sized specimens are necessarily influenced by boundary conditions at the edges, we also investigated the stability of infinite periodic triangular lattices. Since buckling may alter the periodicity of the structure, we considered super cells consisting of $m \times n$ undeformed unit cells subjected to periodic boundary conditions and calculated the critical strain for each of them. The critical strain of the infinite periodic structure is then defined as the minimum critical strain on all considered super cells. The results confirmed those of the finite
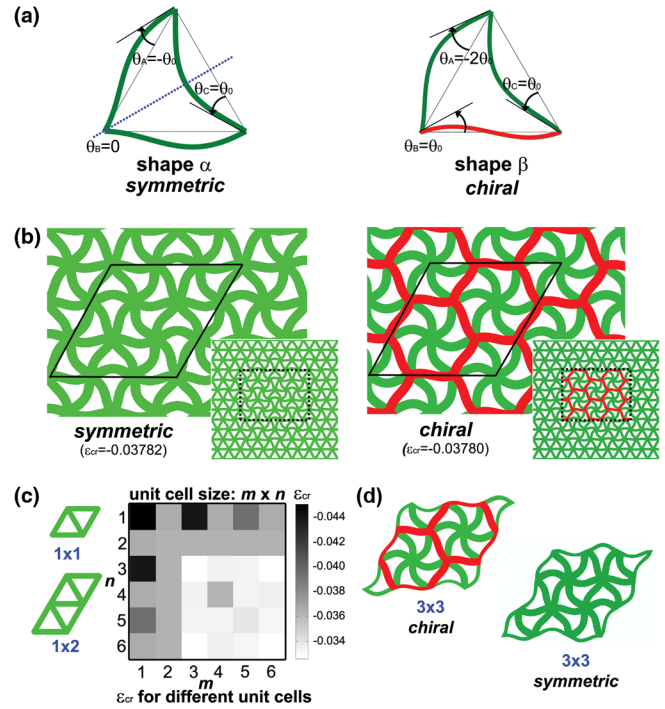

FIG. 2 (color online). Analytical and numerical modeling. (a) Representative critical eigenmodes obtained from the buckling analysis of a single triangular frame. The dotted line indicates the mirror plane for the symmetric pattern. The beam that buckles into a full sinusoid is indicated in red. (b) First and second eigenmodes obtained from the finite element analysis for a lattice structure comprising 11×12 unit cells under equibiaxial compression. The frame is constructed from beams with thickness (t) to length (L) ratio of 0.2. Note that the eigenvalues associated with the two modes are very close to each other. Both the full structures and the magnified views of their central regions are shown. (c) Critical strain for super cells with $t/L = 0.2$ consisting of $m \times n$ unit cells, where a unit cell consists of two adjacent triangles. In the analysis, we used periodic boundary conditions to eliminate edge effects. The results indicate that the 3×3 configuration has the minimum critical strain. (d) Two buckling patterns (one symmetric and one chiral) are associated with the critical strain of the 3×3 configuration. For the chiral pattern, the mirror image of the pattern can also appear.

size simulations and showed that the 3×3 configuration has the minimum critical strain with two possible eigenmodes [Figs. 2(c) and 2(d) and Tables S4 and S5].

To investigate the origin of the ordered patterns induced by buckling in our frustrated system, we introduced a spin-like model. Our goal is to construct a simple model for estimating the energy associated with different spin configurations corresponding to buckled beams, and for identifying the minimum energy configurations. Since in two dimensions a beam can buckle "up" or "down," we represent its buckling direction with an Ising-like unit spin vector $\mathbf{s}_i$ [see Fig. 3(a)]. Such spins are placed at the centers of prebuckled beams, forming the well-known kagome lattice [25,26]. For the sake of simplicity, we first consider

the case where every beam buckles into a half sinusoid so that the energy difference between configurations comes from changes in relative orientation at the joints (i.e., at triangle corners). Here, the deformation of the $\pi/3$ angle between neighboring beams is associated with the energy cost $J_1 > 0$. Therefore, the total energy of a buckled configuration is given by

$$E = -\sum_{\langle i,j \rangle} J_1(\mathbf{s}_i \cdot \mathbf{s}_j - 1/2), \quad (2)$$

where $\mathbf{s}_i$ and $\mathbf{s}_j$ are two nearest neighbor spins [e.g., purple arrows with respect to the reference spin in Fig. 3(a)]. Such antiferromagnetic spin model on the kagome lattice has been studied extensively [25,26]. For a structure comprising N triangles, the minimum energy configurations correspond to a tiling with N buckled units α from Fig. 2(a) ($E_{\min} = NJ_1$), and it has been shown that there are exponentially many ground states due to geometric frustration [25,26]. Therefore, we find exponentially many disordered tilings [e.g., see Fig. 3(b)] and only a small number of ordered tilings, one of which corresponds to the symmetric ordered pattern observed in the numerical analysis [Fig. 3(c)].

However, the finite element simulations described above are favoring ordered structures. The reason for this might be interactions among neighboring triangles coupled through joints. To take this into account, we consider the second nearest neighbor interactions between spins [see Fig. 3(a)] and assign an energy cost $J_2(0 < J_2 \ll J_1)$ to connected beams that deform the $2\pi/3$ angle. For simplicity, we assume that the energy costs of deformations of $\pi/3$ and $2\pi/3$ angles at joints are additive, so that

$$E = -\sum_{\langle i,j \rangle} J_1(\mathbf{s}_i \cdot \mathbf{s}_j - 1/2) + \sum_{\langle k,l \rangle} J_2(\mathbf{s}_k \cdot \mathbf{s}_l + 1/2), \quad (3)$$

where $\mathbf{s}_k$ and $\mathbf{s}_l$ are pairs of second nearest neighbor spins [e.g., blue arrows with respect to the reference spin in Fig. 3(a)] and J_1 and J_2 are positive quantities, since any elastic deformation is associated with a positive energy cost. This additional interaction breaks the degeneracy, so that the symmetric ordered configuration shown in Fig. 3(c) is the only one that minimizes the energy given in Eq. (3) [26]. Our findings nicely agree with previous observations reported for antiferromagnetic systems [7] where additional interactions (often long ranged) are needed for ordered ground states to emerge. Moreover, it is worth noting that for this ordered symmetric pattern we find a striking correlation between its arrangement of spins and that of the ideal spin solid [9].

The spinlike model described above can also be generalized to allow for a second buckling mode of the beams, which is associated with the energy cost Δ. This is achieved by assigning two spins to each beam, where aligned
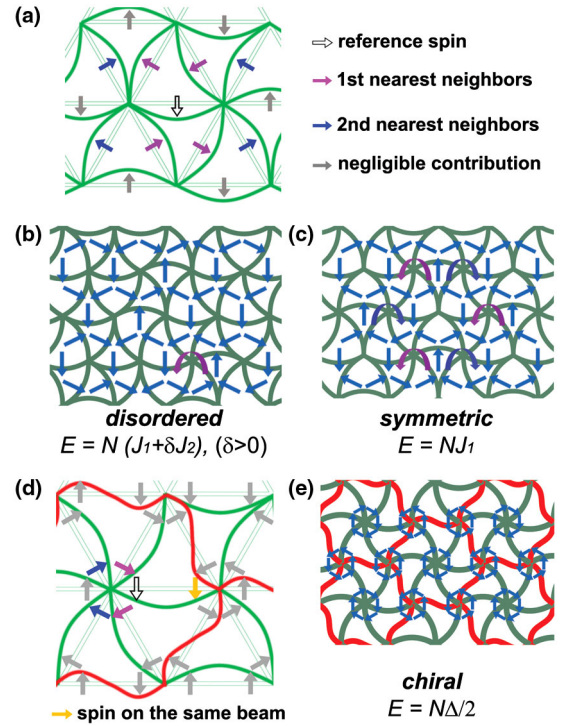

FIG. 3 (color online). Spin-like model. (a) A schematic showing how spins define a buckled pattern when all of the beams buckle into a half sinusoid. (b) Disordered and (c) ordered symmetric configurations predicted by the model. When considering only first nearest neighbor interactions (i.e., $J_2 = 0$), there are exponentially many disordered tilings that minimize the energy for a lattice structure with N triangles and only a small number of ordered patterns. However, only the symmetric ordered configuration minimizes the energy if second nearest neighbor interactions are considered (i.e., $J_2 > 0$). (d) The spinlike model can be generalized to allow for the second buckling mode of the beams by assigning two spins to each beam. (e) A new chiral ordered state emerges when two spins are assigned to each beam. Again, the mirror image of the chiral pattern can also appear.

and antialigned spins correspond to the first and second buckling mode, respectively [see Fig. 3(d)]. The energy cost of a buckled configuration can then be calculated as

$$E = -\sum_{\langle i,j \rangle} J_1(\mathbf{s}_i \cdot \mathbf{s}_j - 1/2) + \sum_{\langle k,l \rangle} J_2(\mathbf{s}_k \cdot \mathbf{s}_l + 1/2)$$
$$- \sum_{\langle m,n \rangle} \frac{\Delta}{2}(\mathbf{s}_m \cdot \mathbf{s}_n - 1), \quad (4)$$

where $\mathbf{s}_m$ and $\mathbf{s}_n$ are two spins assigned to the same beam. In this case, in addition to the ordered configuration described above [Fig. 3(c)], a new chiral ordered state emerges [Fig. 3(e)], which can be constructed from tiling the plane with the buckled triangular unit β from Fig. 2(a). This chiral configuration preserves both the first and the second nearest angles at joints and is associated with the

energy cost $N\Delta/2$, where the factor 1/2 comes from sharing the second mode buckled beam between two triangles. Thus, when $\Delta/2 > J_1$, the minimum energy configuration is the symmetric one [Fig. 3(c)], while when $\Delta/2 < J_1$ it is the chiral one [Fig. 3(e)].

Next, we conduct a simple scaling analysis to determine how the parameters J_1, J_2, and Δ depend on the geometry of the beams (thickness t, length L, and out-of-plane height h) and the elastic property of the material (Young's modulus E). We start by noting that the buckled shape of a thin beam ($t \ll L$) can be well approximated by [27]

$$y(s) = A_m \sin\left(\frac{m\pi s}{L}\right), \tag{5}$$

where m is an integer representing the buckling mode and s is the intrinsic length parameter of the beam, $s \in [0, L]$. It follows that y' and y'' scale as

$$y' \sim A_m \frac{m}{L}, \qquad y'' \sim A_m \frac{m^2}{L^2}. \tag{6}$$

Furthermore, the amplitude A_m can be related to the small compressive strain $\varepsilon \ll 1$ by considering that the beam is inextensible (i.e., $ds^2 = dx^2 + dy^2$), so that

$$
\begin{aligned}
L(1 - \epsilon) &= \int_0^L dx \\
&= \int_0^L ds \sqrt{1 - (y')^2} \approx L\left(1 - \frac{m^2\pi^2 A_m^2}{4L^2}\right).
\end{aligned} \tag{7}
$$

By comparing the left and right sides of Eq. (7) we find

$$A_m \sim \sqrt{\epsilon}(L/m). \tag{8}$$

An estimate for the energy cost Δ associated with the beam buckling into the second mode can then be obtained using elastic plate theory and approximating the bending energy of the buckled beam as

energy $\sim$ plate area $\times$ bending rigidity $\times$ (curvature $\sim y''$)^2,

$$\text{energy} \sim Lh \times Et^3 \times \frac{\varepsilon m^2}{L^2}, \tag{9}$$

so that

$$\Delta \sim \epsilon Eht^3/L. \tag{10}$$

In a similar way, we can estimate the energy cost J_1 and J_2 for deforming the $\pi/3$ and $2\pi/3$ angles between neighboring beams at joints. Since these deformations are localized near joints and only affect a beam region of length $\sim t$, we have

$J_1, J_2 \sim$ volume $\times$ elastic constant $\times$ (local strain $\sim y'$)^2,

$$J_1, J_2 \sim ht^2 \times E \times \epsilon = \epsilon Eht^2. \tag{11}$$

From the scaling analysis above we find that Δ/J_1 scales as t/L, indicating the opportunity to tune the formation of the symmetric or chiral pattern by controlling the beam aspect ratio. In fact, we expect that the chiral and symmetric patterns emerge for small and large t/L, respectively, and numerical FE simulations predict a sharp first-order-like transition at $t/L \approx 0.24$ [see Table S6]. Finally, it is worth noting that the chiral pattern arises with a new spin configuration, thus, highlighting the richness of our frustrated system.

Guided by our theoretical analysis, we fabricated centimeter scale elastomeric triangular cellular structures with $t/L = 0.2$ and 0.3 ($L = 5$ mm) comprising 11×12 unit cells [Figs. 4(a) and 4(b), left]. The experimental results show an excellent agreement with the analytical and numerical predictions. When tested under equibiaxial compression, we, indeed, observed the formation of an ordered chiral pattern for $t/L = 0.2$ [Fig. 4(a), center and right]. Moreover, as predicted by the scaling analysis, an ordered symmetric pattern emerged for $t/L = 0.3$ [Fig. 4(b), center and right]. Since geometrical frustration in our continuum system is induced by a mechanical instability that is scale independent (where the continuum assumption holds), our findings can be extended to different length scales, materials, and stimuli. In fact, similar patterns were also observed by swelling surface-attached triangular cellular structures [Fig. S5], providing us opportunities to study the effects of kinetics on geometrical frustration.
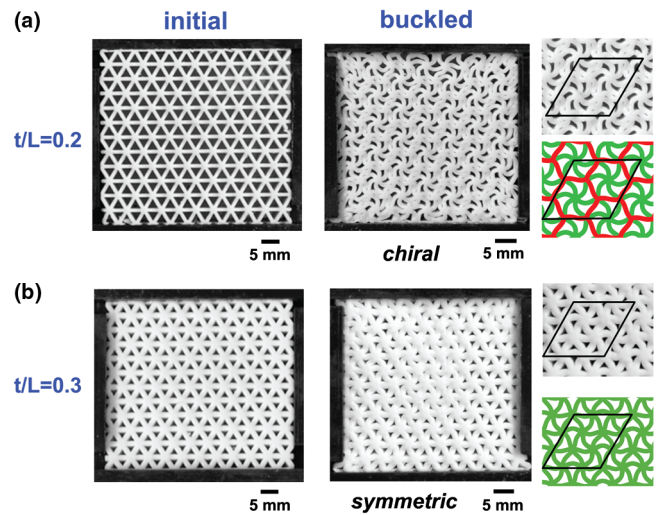

FIG. 4 (color online). Experimental observation of ordered chiral or symmetric patterns. (a), (b) Initial and buckled configurations (at $\epsilon = 0.16$) for a sample characterized by $t/L = 0.2$ and $t/L = 0.3$ ($L = 5$ mm), respectively. The insets on the right show magnified images of the buckled patterns obtained experimentally and numerically.

In summary, we have studied analytically, numerically, and experimentally geometrical frustration induced by buckling in continuum triangular cellular structures. Interestingly, we found that the connected geometry favors the formation of complex ordered symmetric or chiral patterns, and the appearance of a specific configuration is controlled by the porosity of the system. In stark contrast to most of the artificial frustrated systems previously studied, ordered configurations emerge naturally in our structures, indicating that the coupling between elasticity and geometrical frustration in continuum structures opens the door to a new class of phenomena waiting to be explored. In fact, while the symmetric pattern induced by buckling has a striking correlation with the arrangement of spins in the ideal spin solid, no analogous spin arrangement to that of our chiral configuration has been reported. Our results also indicate that simple changes in the geometry of the elastic structures may lead to novel effects that can be easily visualized, since—unlike for the case of magnetic systems—our experimental system can be quickly fabricated and tested. With their intriguing and rich behavior originating from the interplay between geometry and deformation, continuum geometrically frustrated lattice structures offer many novel phenomena to be investigated.

---

[*]Corresponding author.
bertoldi@seas.harvard.edu

[1] J.-F. S. Sadoc and R. Mosseri, *Geometrical Frustration* (Cambridge University Press, Cambridge, England, 2006).

[2] Y. Han, Y. Shokef, A. M. Alsayed, P. Yunker, T. C. Lubensky, and A. G. Yodh, Nature (London) **456**, 898 (2008).

[3] L. Balents, Nature (London) **464**, 199 (2010).

[4] R. F. Wang, C. Nisoli, R. S. Freitas, J. Li, W. McConville, B. J. Cooley, M. S. Lund, N. Samarth, C. Leighton, V. H. Crespi, and P. Schiffer, Nature (London) **439**, 303 (2006).

[5] Y. Qi, T. Brintlinger, and J. Cumings, Phys. Rev. B **77**, 094418 (2008).

[6] P. E. Lammert, X. Ke, J. Li, M. Khan, C. Nisoli, D. M. Garand, V. H. Crespi, and P. Schiffer, Nat. Phys. **6**, 786 (2010).

[7] S. A. Daunheimer, O. Petrova, O. Tchernyshyov, and J. Cumings, Phys. Rev. Lett. **107**, 167201 (2011).

[8] J. P. Morgan, A. Stein, S. Langridge, and C. H. Marrows, Nat. Phys. **7**, 75 (2011).

[9] W. R. Branford, S. Ladak, D. E. Read, K. Zeissler, and L. F. Cohen, Science **335**, 1597 (2012).

[10] A. Farhan, P. M. Derlet, A. Kleibert, A. Balan, R. V. Chopdekar, M. Wyss, L. Anghinolfi, F. Nolting, and L. J. Heyderman, Nat. Phys. **9**, 375 (2013).

[11] S. Zhang, I. Gilbert, C. Nisoli, G.-W. Chern, M. J. Erickson, L. O'Brien, C. Leighton, P. E. Lammert, V. H. Crespi, and P. Schiffer, Nature (London) **500**, 553 (2013).

[12] Y. Shokef and T. C. Lubensky, Phys. Rev. Lett. **102**, 048303 (2009).

[13] P. Yunker, Z. Zhang, and A. G. Yodh, Phys. Rev. Lett. **104**, 015701 (2010).

[14] P. Mellado, A. Concha, and L. Mahadevan, Phys. Rev. Lett. **109**, 257203 (2012).

[15] M. J. Harris, S. T. Bramwell, D. F. McMorrow, T. Zeiske, and K. W. Godfrey, Phys. Rev. Lett. **79**, 2554 (1997).

[16] R. Siddharthan, B. S. Shastry, A. P. Ramirez, A. Hayashi, R. J. Cava, and S. Rosenkranz, Phys. Rev. Lett. **83**, 1854 (1999).

[17] B. C. den Hertog and M. J. P. Gingras, Phys. Rev. Lett. **84**, 3430 (2000).

[18] C. Lobban, J. L. Finney, and W. F. Kuhs, J. Chem. Phys. **112**, 7169 (2000).

[19] C. Salzmann, P. Radaelli, A. Hallbrucker, E. Mayer, and J. Finney, Science **311**, 1758 (2006).

[20] Z.-Y. Chen and M. Kardar, J. Phys. C **19**, 6825 (1986).

[21] L. Gu, B. Chakraborty, P. L. Garrido, M. Phani, and J. L. Lebowitz, Phys. Rev. B **53**, 11985 (1996).

[22] S. Singamaneni and V. V. Tsukruk, Soft Matter **6**, 5681 (2010).

[23] M. Gregory, *Elastic Instability: Analysis of Buckling Modes and Loads of Framed Structures* (Taylor and Francis, London, 1967).

[24] See Supplemental Material at http://link.aps.org/supplemental/10.1103/PhysRevLett.112.098701 for details on analysis and experiments.

[25] R. Liebmann, *Statistical Mechanics of Periodic Frustrated Ising Systems* (Springer-Verlag, Berlin, 1986), pp. 77–81.

[26] A. S. Wills, R. Ballou, and C. Lacroix, Phys. Rev. B **66**, 144407 (2002).

[27] S. P. Timoshenko and J. M. Gere, *Theory of Elastic Stability* (Courier Dover Publications, New York, 2012).

Supporting Information for Complex ordered patterns in mechanical instability induced geometrically frustrated triangular cellular structures

Sung Hoon Kang,[1] Sicong Shan,[1] Andrej Košmrlj,[2] Wim L. Noorduin,[1]
Samuel Shian,[1] James C. Weaver,[3] David R. Clarke,[1] and Katia Bertoldi[1,4]

[1]School of Engineering and Applied Sciences, Harvard University, Cambridge, Massachusetts 02138, USA
[2]Department of Physics, Harvard University, Cambridge, Massachusetts 02138, USA
[3]Wyss Institute for Biologically Inspired Engineering,
Harvard University, Cambridge, Massachusetts 02138, USA
[4]Kavli Institute, Harvard University, Cambridge, Massachusetts 02138, USA
(Dated: January 21, 2014)

STABILITY OF A TRIANGULAR FRAME

Here we investigate analytically the stability of a single triangular frame consisting of three elastic beams of bending stiffness EI and length L, rigidly connected to each other, so that their relative orientation is fixed. Assuming that the beams are slender so that the contribution of the shear forces can be neglected, we use the stiffness matrix of a beam-column[1, 2] and impose equilibrium conditions at each joint to determine the critical load and the corresponding modes.

We start by recalling that the response of an initially straight elastic beam AB with bending stiffness EI and length L subject to an axial load P and end moments M_A and M_B (see Fig. 1) is described by[1]

$$\frac{d^2y}{dx^2} + \frac{P}{EI}\, y = -\frac{M_A}{EI}\left(1 - \frac{x}{L}\right) + \frac{M_B}{EI\, L}\, x, \tag{1}$$

where x and $y(x)$ denote the distance and the lateral displacement along the beam, respectively.
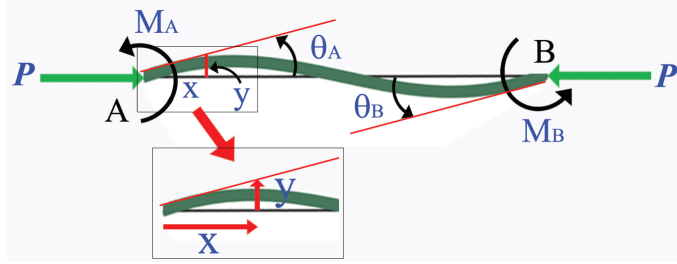

FIG. 1: **Schematic of a beam under compression.**

The solution of the Eq. (1) is given by

$$y = A\sin(k\,x) + B\cos(k\,x) - \frac{M_A}{P}\left(1 - \frac{x}{L}\right) + \frac{M_B}{P}\frac{x}{L}, \tag{2}$$

where $k^2 = P/EI$. The coefficients A and B in Eq. (2) can be obtained by imposing the boundary conditions $y(0) = y(L) = 0$, yielding

$$B = \frac{M_A}{P}, \quad \text{and} \quad A = -\frac{M_A}{P}\cot(k\,L) - \frac{M_B}{P}\csc(kL). \tag{3}$$

After substitution of Eqs. (3) into Eq. (2) the slope at the two ends A and B can be calculated as

$$\theta_A = y'(0) = \frac{1}{EI}\left(M_A L\,\beta + M_B L\,\alpha\right), \quad \text{and} \quad \theta_B = y'(L) = \frac{1}{EI}\left(M_B L\,\beta + M_A L\,\alpha\right), \tag{4}$$

with

$$\alpha = \frac{1}{k^2 L^2}(1 - kL\csc kL), \quad \beta = \frac{1}{k^2 L^2}(1 - kL\cot kL). \tag{5}$$

It is often convenient to invert Eqs. (4), yielding

$$M_A = \frac{EI}{L}\left(\frac{\beta}{\beta^2 - \alpha^2}\theta_A + \frac{\alpha}{\alpha^2 - \beta^2}\theta_B\right) = \frac{EI}{L}\left(S\theta_A + SC\theta_B\right),$$

$$M_B = \frac{EI}{L}\left(\frac{\alpha}{\alpha^2 - \beta^2}\theta_A + \frac{\beta}{\beta^2 - \alpha^2}\theta_B\right) = \frac{EI}{L}(SC\theta_A + S\theta_B)$$

(6)

where

$$S = \frac{(1 - kL\cot kL)kL}{2\tan(\frac{1}{2}kL) - kL}, \quad C = \frac{kL\csc kL - 1}{1 - kL\cot kL}.$$

(7)

Next we consider an equilateral triangular frame with all beams compressed by an axial force P, as shown in Fig. 2. In this case Eqs. (6) specialize to

$$M_{AB} = \frac{EI}{L}(S\theta_{AB} + SC\theta_{BA}), \qquad M_{AC} = \frac{EI}{L}(S\theta_{AC} + SC\theta_{CA}),$$

$$M_{BA} = \frac{EI}{L}(S\theta_{BA} + SC\theta_{AB}), \qquad M_{BC} = \frac{EI}{L}(S\theta_{BC} + SC\theta_{CB}),$$

$$M_{CA} = \frac{EI}{L}(S\theta_{CA} + SC\theta_{AC}), \qquad M_{CB} = \frac{EI}{L}(S\theta_{CB} + SC\theta_{BC}),$$
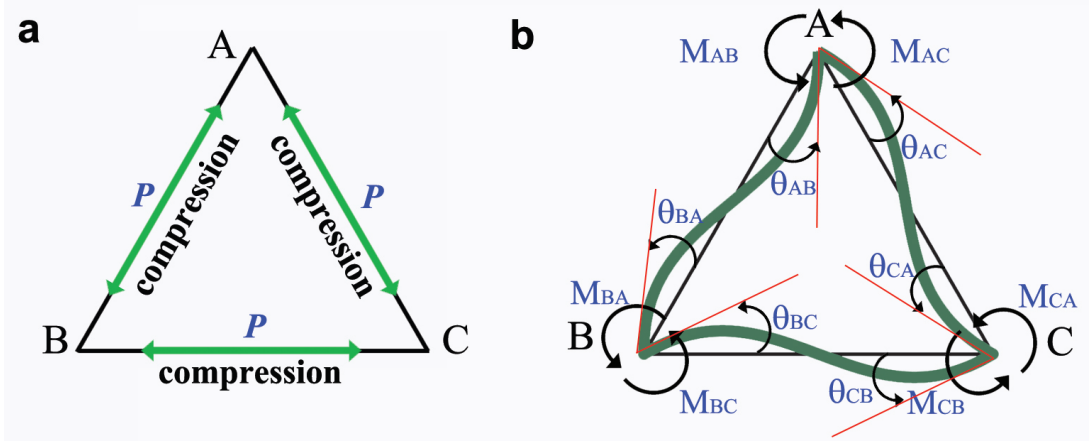
(8)

FIG. 2: **Schematic of a triangular frame under equibiaxial compression. a,** A compressive load P was applied to all three beams with length L and bending stiffness EI. **b,** Buckling of a triangular frame.

Since we consider beams that are rigidly connected to each other, $\theta_{AB} = \theta_{AC} = \theta_A$, $\theta_{BA} = \theta_{BC} = \theta_B$ and $\theta_{CA} = \theta_{CB} = \theta_C$. Also, since there are no applied external moments at the joints, equilibrium requires that $M_{AB} = -M_{AC}$, $M_{BA} = -M_{BC}$, $M_{CB} = -M_{CA}$. Therefore, Eqns. (8) reduce to

$$\begin{aligned}(S\theta_A + SC\theta_B) + (S\theta_A + SC\theta_C) &= 0,\\ (S\theta_B + SC\theta_A) + (S\theta_B + SC\theta_C) &= 0,\\ (S\theta_C + SC\theta_A) + (S\theta_C + SC\theta_B) &= 0,\end{aligned}$$

(9)

which can be rewritten in matrix form as

$$\begin{pmatrix} 2S & SC & SC \\ SC & 2S & SC \\ SC & SC & 2S \end{pmatrix}\begin{pmatrix} \theta_A \\ \theta_B \\ \theta_C \end{pmatrix} = \begin{pmatrix} 0 \\ 0 \\ 0 \end{pmatrix}.$$

(10)

Non-trivial solutions exist when the determinant of the matrix (i.e. the *stiffness matrix*) in Eq. (10) is zero,

$$S^3(C^3 - 3C^2 + 4) = S^2(C - 2)^2(C + 1) = 0.$$

(11)

Since $S = 0$ yields only trivial solutions, it is easy to see that Eq. (11) is satisfied when

- (i) $(C - 2) = 0$, so that

$$\frac{kL \csc kL - 1}{1 - kL \cot kL} = 2, \tag{12}$$

from which kL can be solved numerically, yielding $kL \sim 3.8567$. Therefore, the corresponding critical load is given by

$$P_{cr,1} = k^2 EI = \left(\frac{3.8567}{L}\right)^2 EI \sim 14.87 \frac{EI}{L^2}. \tag{13}$$

Moreover, the corresponding eigenmode can be obtained by substituting $C = 2$ into Eq. (10), yielding

$$\theta_A + \theta_B + \theta_C = 0. \tag{14}$$

- (ii) $(C + 1) = 0$, so that

$$\frac{kL \csc kL - 1}{1 - kL \cot kL} = -1, \tag{15}$$

from which kL can be solved numerically, yielding $kL \sim 5.1362$. Therefore, the corresponding critical load is given by

$$P_{cr,2} = k^2 EI = \left(\frac{5.1362}{L}\right)^2 EI \sim 26.38 \frac{EI}{L^2}, \tag{16}$$

and the corresponding eigenmode is

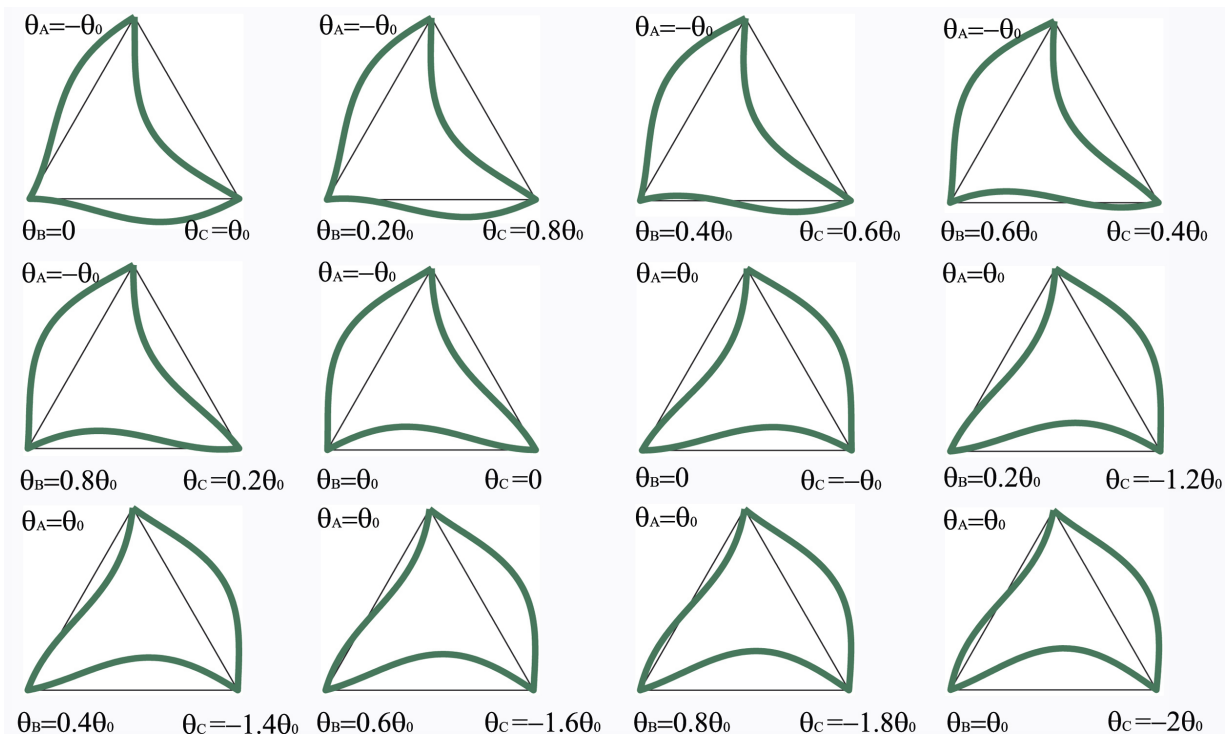$$\theta_A = \theta_B = \theta_C. \tag{17}$$

FIG. 3: **Examples of critical eigenmodes.** θ_0 is used as reference angle.

Therefore, the analysis indicates that the frame buckles when $P = P_{cr,1} = P_{cr} \sim 14.87 \frac{EI}{L^2}$ and that buckling introduces degeneracy, since there are an infinite number of modes satisfying Eq. (14), some of which are shown in

Fig. 3. Note that these modes have been obtained by substituting the critical load and corresponding eigenmode into Eq. (2) and that they include also the symmetric pattern with $\theta_B = 0$ and $\theta_A = -\theta_C$ and the chiral configuration with $\theta_A = -2\theta_C$ and $\theta_B = \theta_C$ shown in Fig. 2-a in the main text.

Finally it is worth noting that buckling does not induce geometrical frustration in both (i) triangular frames with rigid junctions compressed uniaxially and (ii) triangular frames with free-to-rotate junctions compressed equibiaxially. In fact, for a triangular frame uniaxially compressed buckling occurs when $P = 16EI/L^2$ leading to a mode for which $\theta_A = \theta_B = \theta_C$ [1]. Moreover, when the beams at the junctions are free-to-rotate the frame buckles when $P = P_{cr} = \pi^2 \frac{EI}{L^2}$, leading to a mode in which each beam buckles into a perfect half-sinusoid.

STABILITY OF A TRIANGULAR CELLULAR STRUCTURE SUBJECTED TO EQUIBIAXIAL COMPRESSION

To investigate the patterns induced by buckling in triangular cellular structures, we investigated numerically the stability of finite size and infinite periodic samples subjected to equibiaxial compression using the commercial finite element package Abaqus 6.11. We built 2D models using quadratic plain strain elements (Abaqus type CPE8H and CPE6H) and modeled the material using an almost incompressible Neo-Hookean hyper-elastic model[3] with initial bulk modulus $K_0 = 100 \mu_0$, μ_0 denoting the initial shear modulus. The accuracy of each mesh was ascertained through a mesh refinement study.

Finite size structures.

We considered finite size structures in which each triangle has the same dimensions as in the experiments (i.e. length $L = 5$ mm and thickness $t \in [0.025, 1.625]$ mm) and we investigated their stability using eigenvalue analysis. To simulate the experimental test conditions the bottom and left edges were fixed in the vertical and horizontal direction, respectively, whereas the top and right edges were uniformly compressed in the vertical and horizontal direction, respectively. A linear perturbation procedure was used and was accomplished within the commercial finite element code ABAQUS/Standard using the *BUCKLE module. Eigen analysis of the unloaded structures and of the structures after application of a modest compression yielded very similar results. The analysis yielded the transformed pattern (the eigenmode) and the critical nominal strain (the eigenvalue).

We started by investigating the stability of a structure with the same size as that used in the experiments (i.e. 11×12 unit cells composed of two adjacent triangles - see Fig. 2c in the main text). The results reported in the Fig. 2b of the main text show that there are two buckling patterns (symmetric and chiral) with very close energy states ($\epsilon_{cr}^{chiral} = -0.03780$ and $\epsilon_{cr}^{sym} = -0.03782$). The symmetric pattern consists of the symmetric buckled units (α) from our analytical study and the chiral pattern consist of the chiral units (β). Interestingly, both patterns are characterized by a periodic unit comprising 3×3 undeformed unit cells.

To make sure the response of the structure is not influenced by size effects, we investigated the stability of structures with $t/L = 0.2$ comprising of a different number of unit cells. We find that all the structures are characterized by two very close eigenvalues (see Table I) associated to the symmetric and chiral patterns shown in Fig. 2b of the main text. The simulated samples had up to 51×50 unit cells and we did not found any significant size effect.

Next, we investigated the effect of the wall aspect ratio t/L on the stability of structures comprising of 5×6 and 11×12 unit cells. The results reported in Tables II and III indicate that the critical strain values are similar between the two patterns regardless of the geometrical parameter t/L.

TABLE I: Critical strains associated to the chiral and symmetric pattern for finite size structures with with $t/L = 0.2$ comprising $m \times n$ unit cells.

m	n	ϵ_{cr}^{chiral}	ϵ_{cr}^{sym}
6	6	-4.239×10^{-2}	-4.307×10^{-2}
8	6	-4.136×10^{-2}	-4.070×10^{-2}
6	8	-4.156×10^{-2}	-4.257×10^{-2}
7	7	-4.091×10^{-2}	-4.150×10^{-2}
10	6	-3.999×10^{-2}	-4.027×10^{-2}
8	8	-4.070×10^{-2}	-4.010×10^{-2}
10	8	-3.938×10^{-2}	-3.959×10^{-2}
9	9	-3.957×10^{-2}	-3.978×10^{-2}
8	12	-4.020×10^{-2}	-3.954×10^{-2}
12	8	-3.900×10^{-2}	-3.906×10^{-2}
10	10	-3.914×10^{-2}	-3.929×10^{-2}
14	8	3.879×10^{-2}	-3.869×10^{-2}
11	11	-3.897×10^{-2}	-3.873×10^{-2}
12	12	-3.853×10^{-2}	-3.860×10^{-2}
13	13	-3.822×10^{-2}	-3.843×10^{-2}
18	10	-3.812×10^{-2}	-3.813×10^{-2}
20	10	-3.805×10^{-2}	-3.801×10^{-2}
18	12	-3.797×10^{-2}	-3.798×10^{-2}
15	15	-3.804×10^{-2}	-3.807×10^{-2}
16	16	-3.792×10^{-2}	-3.797×10^{-2}
22	12	-3.780×10^{-2}	-3.782×10^{-2}
51	50	-3.406×10^{-2}	-3.405×10^{-2}

TABLE II: Critical strains associated to the chiral and symmetric pattern for finite size structures with 5×6 unit cells and different aspect ratios t/L.

t/L	ϵ_{cr}^{chiral}	ϵ_{cr}^{sym}
0.050	-3.120×10^{-3}	-3.143×10^{-3}
0.075	-6.789×10^{-3}	-6.840×10^{-3}
0.100	-1.167×10^{-2}	-1.175×10^{-2}
0.125	-1.759×10^{-2}	-1.772×10^{-2}
0.150	-2.441×10^{-2}	-2.458×10^{-2}
0.175	-3.194×10^{-2}	-3.215×10^{-2}
0.200	-3.999×10^{-2}	-4.023×10^{-2}
0.225	-4.831×10^{-2}	-4.859×10^{-2}
0.250	-5.684×10^{-2}	-5.720×10^{-2}
0.275	-6.559×10^{-2}	-6.592×10^{-2}
0.300	-7.956×10^{-2}	-7.955×10^{-2}
0.325	-8.494×10^{-2}	-8.540×10^{-2}
0.350	-9.006×10^{-2}	-9.211×10^{-2}

TABLE III: Critical strains associated to the chiral and symmetric pattern for finite size structures with 11×12 unit cells and different aspect ratios t/L.

t/L	ϵ_{cr}^{chiral}	ϵ_{cr}^{sym}
0.050	-2.967×10^{-3}	-2.968×10^{-3}
0.100	-1.104×10^{-2}	-1.105×10^{-2}
0.150	-2.316×10^{-2}	-2.317×10^{-2}
0.200	-3.780×10^{-2}	-3.782×10^{-2}
0.250	-5.395×10^{-2}	-5.397×10^{-2}
0.275	-6.239×10^{-2}	-6.245×10^{-2}
0.300	-7.378×10^{-2}	-7.378×10^{-2}

Infinite periodic structures.

Recognizing that the finite-sized specimens are necessarily influenced by boundary conditions at the edges, we also investigated the stability of infinite periodic triangular lattices. Taking as primitive cell two adjacent triangles (as shown in Fig. 3c of the main text), the infinite periodic structure is modeled as representative volume elements (RVEs) consisting of $m \times n$ cells subjected to periodic boundary conditions. The critical strain of the infinite periodic structure is then defined as the minimum of ϵ_{cr} on all possible periodic RVEs. In Fig. 2c of the main text and in Tables IV and V we report the critical strains for periodic RVE with $m \times n$ cells for both $t/L = 0.2$ and 0.3. The results indicate that the critical strain is minimum for the periodic unit comprising 3×3 unit cells and that there are two possible eigenmodes (one chiral and one symmetric, as shown in Fig. 3d of the main text) associated to it. Therefore, this analysis confirm the results of the finite size simulations and show that the 3×3 configuration has the minimum critical strain.

Finally, since our scaling analysis shows that Δ/J_1 scales as t/L and indicates the opportunity to tune the formation of the symmetric or chiral pattern by controlling the beam aspect ratio t/L, we used FE simulations to study this transition. In particular, we considered a super-cell consisting of 3×3 undeformed unit cells subjected to periodic boundary conditions and numerically calculated its critical strain for increasing values of t/L. As shown in Table VI, we find that the chiral and symmetric patterns emerge for $t/L \leq 0.235$ and $t/L > 0.235$, respectively. Therefore, $t/L = 0.235$ marks a sharp transition from the chiral to the symmetric pattern.

TABLE IV: Critical strains for periodic RVEs of different size with $t/L = 0.2$.

m× n	1	2	3	4	5	6
1	-6.982×10^{-2}	-3.659×10^{-2}	-4.381×10^{-2}	-3.663×10^{-2}	-3.936×10^{-2}	-3.659×10^{-2}
2	-3.659×10^{-2}	-3.626×10^{-2}	-3.626×10^{-2}	-3.629×10^{-2}	-3.628×10^{-2}	-3.628×10^{-2}
3	-4.381×10^{-2}	-3.626×10^{-2}	-3.255×10^{-2}	-3.350×10^{-2}	-3.338×10^{-2}	-3.255×10^{-2}
4	-3.663×10^{-2}	-3.629×10^{-2}	-3.350×10^{-2}	-3.624×10^{-2}	-3.344×10^{-2}	-3.357×10^{-2}
5	-3.936×10^{-2}	-3.628×10^{-2}	-3.338×10^{-2}	-3.344×10^{-2}	-3.395×10^{-2}	-3.334×10^{-2}
6	-3.659×10^{-2}	-3.628×10^{-2}	-3.255×10^{-2}	-3.357×10^{-2}	-3.334×10^{-2}	-3.255×10^{-2}

TABLE V: Critical strains for periodic RVEs of different size with $t/L = 0.3$

m× n	1	2	3	4	5	6
1	-1.412×10^{-1}	-8.000×10^{-2}	-9.375×10^{-2}	-8.000×10^{-2}	-8.700×10^{-2}	-8.000×10^{-2}
2	-8.000×10^{-2}	-8.000×10^{-2}	-8.000×10^{-2}	-8.000×10^{-2}	-8.000×10^{-2}	-8.000×10^{-2}
3	-9.375×10^{-2}	-8.000×10^{-2}	-7.100×10^{-2}	-7.300×10^{-2}	-7.320×10^{-2}	-7.100×10^{-2}
4	-8.000×10^{-2}	-8.000×10^{-2}	-7.320×10^{-2}	-8.000×10^{-2}	-7.300×10^{-2}	-7.300×10^{-2}
5	-8.700×10^{-2}	-8.000×10^{-2}	-7.300×10^{-2}	-7.300×10^{-2}	-7.500×10^{-2}	-7.250×10^{-2}
6	-8.000×10^{-2}	-8.000×10^{-2}	-7.100×10^{-2}	-7.300×10^{-2}	-7.300×10^{-2}	-7.100×10^{-2}

TABLE VI: Critical strains for periodic RVEs of different aspect ratios t/L.

t/L	ϵ_{cr}^{chiral}	ϵ_{cr}^{sym}
0.180	-3.0866×10^{-2}	-3.0870×10^{-2}
0.200	-3.6924×10^{-2}	-3.6991×10^{-2}
0.220	-4.3190×10^{-2}	-4.3214×10^{-2}
0.230	-4.6391×10^{-2}	-4.6417×10^{-2}
0.235	-4.8064×10^{-2}	-4.8077×10^{-2}
0.240	-4.9736×10^{-2}	-4.9682×10^{-2}
0.250	-5.3118×10^{-2}	-5.3085×10^{-2}

EXPERIMENTAL TESTS ON FREE-STANDING STRUCTURES

Fabrication.

Macroscale free-standing triangular lattice structures were fabricated by first making negative molds using a 3D printer (Connex 500 available from Objet, Ltd.) with VeroBlue (product number: RGD840, Objet) material and casting positive structures using a silicone rubber (Mold Max 10 from Smooth-On or Elite Double 32 available from Zhermack). Before replication, a releasing agent (Easy Release 200 available from Smooth-On, Inc.) was sprayed on to the molds for easy separation[4]. The casted mixture was first placed in vacuum for degassing and was allowed to set at room temperature for curing. In the free-standing structures each wall/beam has length $L \sim 5$ mm, thickness $t \sim 1$ or 1.5 mm and out-of-plane height $h \sim 10$ mm to minimize out-of-plane buckling.

Buckling-induced pattern formation through equibiaxial compression.

Buckling in the free-standing samples was induced by equibiaxial compression using a custom-built testing setup (see Fig. 4) with four linear actuators (controlled by in-house LabView codes). The resulting patterns were recorded using a Nikon D90 digital SLR camera.
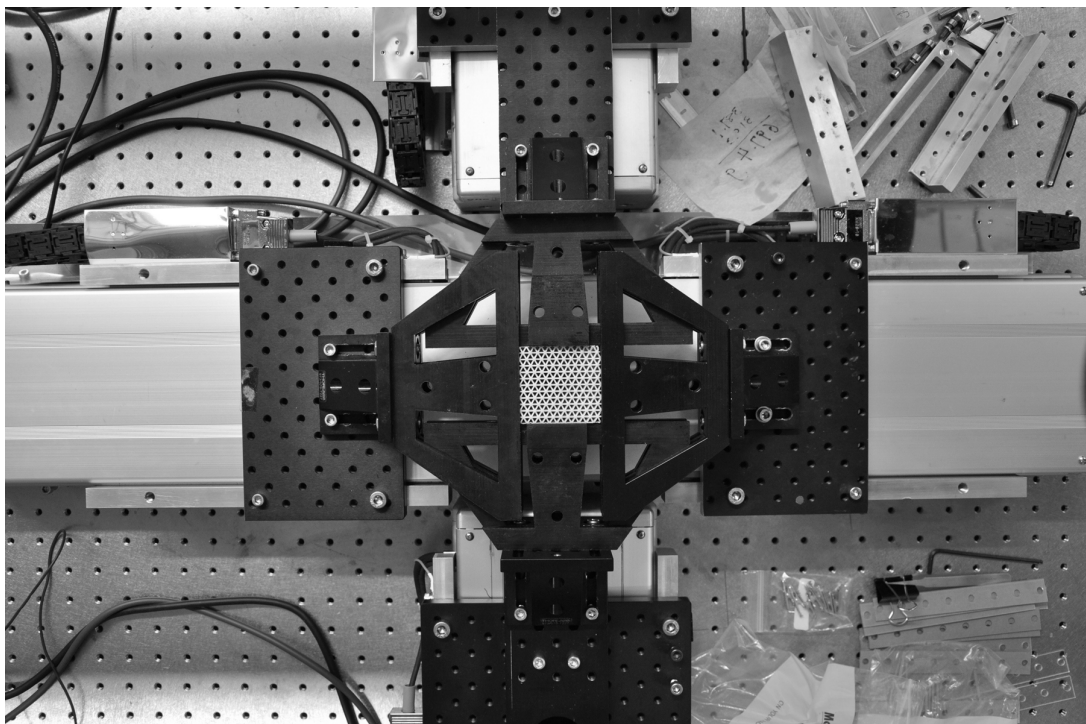

FIG. 4: **The picture of the biaxial compression setup used for our experiments.**

EXPERIMENTAL TESTS ON SURFACE-ATTACHED STRUCTURES

Although in the main text we present results for free-standing triangular cellular structures under equibiaxial compression, similar patterns can also be observed by swelling surface-attached triangular cellular structures.

Fabrication.

Macroscale surface-attached triangular lattice structures were fabricated using the same procedure described above for free-standing structures. Each wall/beam has $L \sim 5$ mm, $t \sim 0.9$ mm, and $h \sim 5$ mm and the lattice structure is attached to a rigid substrate.
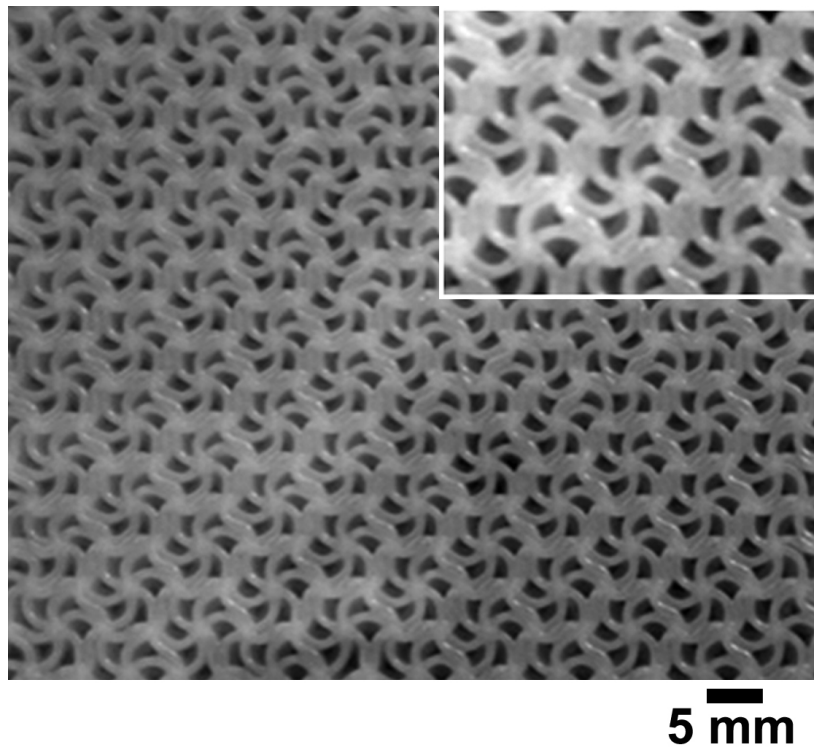

5 mm

FIG. 5: **Buckling of a surface-attached triangular lattice.** The triangular lattice was buckled by immersing the sample in an organic solvent. The inset on the right shows a magnified image of the buckled pattern.

Buckling-induced pattern formation through swelling.

Buckling in the surface-standing samples was induced by swelling using organic solvents such as toluene or hexane (Anhydrous, 99.8% or 95% available from Sigma Aldrich). Buckling occurred due to compressive stresses arising from the geometric constraint that suppresses swelling near the rigid substrate where the structure is clamped. The resulting patterns were recorded using a Nikon D90 digital SLR camera. Fig. 5 shows the buckling pattern induced by swelling in a surface-attached triangular cellular structure, which is very similar to the chiral pattern observed in highly porous free-standing structures under equibiaxial compression.

[1] M. Gregory, *Elastic Instability: Analysis of Buckling Modes and Loads of Framed Structures* (Taylor and Francis, 1967).
[2] Z. P. Bazant and L. Cedolin, *Stability of Structures: Elastic, Inelastic, Fracture, and Damage Theoriess* (Courier Dover Publications, 1981).
[3] R. W. Ogden, *Non-linear Elastic Deformations* (Courier Dover Publications, 1997).
[4] J. Shim, S. Shan, A. Košmrlj, S. H. Kang, E. R. Chen, J. C. Weaver, and K. Bertoldi, Soft Matter **9**, 8198 (2013).